# Sensitivity of GHBMC Lumbar Spine Biomechanical Response to Subject-specific Geometric Morphing and Soft Tissue Material Property Scaling

Sophia K. Tushak, Varun Bollapragada, Cody O'Cain, Jeesoo Shin, Bronislaw D. Gepner, Bengt Pipkorn, Jason R. Kerrigan

***Abstract*** Morphing techniques allow for the incorporation of diverse anthropometries in human body models. In addition, material properties can be adjusted to incorporate the effects of aging. Our objective was to evaluate the effect of subject-specific (SS) geometric morphing and material property scaling on prediction of component lumbar spine biomechanical response in compression-flexion loading. The mesh of the GHBMC-M50 lumbar spine was morphed to SS geometries using CT scans representing pre-test initial positions. Eight specimens were selected, which represented geometry close to and substantially different from the baseline and both males and females. Secondly, soft tissue material properties of the ligaments and intervertebral discs were scaled to determine the effects of increasing or decreasing stiffness. Flexion moment-angle responses were relatively insensitive to changes in geometry and individual changes in soft tissue properties. However, the combined effect of scaling all soft tissues was greater than both individual scaling and morphing. All models captured the experimental response at low sagittal angles, but all models deviated from experiments at higher angles and moments. Given the assessed version of the GHBMC and the applied loading conditions, the effort of incorporating added complexity within the lumbar spine did not substantially alter the measured model outcomes.

***Keywords*** Human body models, lumbar spine injury, spine biomechanics, subject-specific modeling, material scaling.

## I. INTRODUCTION

Lumbar spine injuries continue to occur in frontal motor-vehicle crashes (MVCs) [1-4] and may become more frequent and severe in potential future seating scenarios, as reclining the seat back has been shown to increase lumbar spine loading [5-7]. From concentrated research efforts and fundamental work in lumbar spine injury biomechanics, it has been shown that the lumbar spine is subjected to combined compression-flexion loading when an occupant experiences a frontal MVC [6-9], which can lead to characteristic vertebral body fracture types, such as compression, burst, and wedge fractures [2-3][10-15]. Several human surrogates are utilised to study the causation of, and to predict the risk for, injuries in MVCs, as well as to quantify the human biomechanical response to such loading [16]. Among these physical and virtual surrogates are post-mortem human subjects (PMHS), computational finite element (FE) human body models (HBMs), and anthropometric test devices (ATDs). Specifically, the biomechanical characteristics of HBMs and ATDs, commonly used in MVC scenarios, incorporate PMHS data to achieve human-like behaviour, or biofidelity. HBMs and ATDs are designed to represent one specific anthropometry (baseline [BL] model, e.g. 50$^{th}$ percentile male, 5$^{th}$ percentile female) and optimised or averaged material properties based on different populations, potentially limiting the predictive power of the surrogate. Thus, predictions from a BL model may not be accurate for, nor representative of, any individuals with anatomical and anthropometric characteristics dissimilar to the standard HBM and ATD sizes.

To predict the risk for lumbar spine injury in frontal MVC scenarios, the loads required to produce the aforementioned characteristic injuries were quantified in PMHS [17]. Additionally, the biomechanical responses of the same PMHS were quantified and compared to a widely used BL HBM, in which behavioural differences between the two surrogate responses were illustrated [18]. Incorporating subject-specific (SS) characteristics (geometry or material properties) may improve predictions of biomechanical response to loading, stress state of

S. K. Tushak (e-mail: skt5ay@virginia.edu) is a PhD student in Mechanical Engineering, V. Bollapragada, C. O'Cain, J. Shin, and B. D. Gepner are Research Scientists and J. R. Kerrigan is the Director and Associate Professor in Mechanical Engineering, all at the University of Virginia's Center for Applied Biomechanics, USA. B. Pipkorn is an Adjunct Professor at Chalmers University of Technology, Gothenburg, and Director of Simulation and Active Structures at Autoliv Research, Vårgårda, Sweden.

the tissue, and eventually the risk for certain injuries across broader populations. Several previous studies have highlighted benefits of including SS parameters to improve model predictions of biomechanical response to loading and localised stress/strain measured in PMHS [19-26]. Several studies' authors developed SS models of the bone(s) of interest (ribs [21][23], pelvis [19], clavicle [24], lumbar spine [20][26]), while others morphed the bone(s) of an existing HBM to create SS models that represent each donor's geometry (femur [22], thoracic spine [25]). The former method does not have a BL model in which to compare. The latter method is beneficial because it is usually quicker and more efficient, but it also permits comparison of differences in BL model and SS model predictions, which could assist in determining the necessary level of complexity to achieve convergence in model predictions. For example, Park *et al.*'s [22] illustrated that the error between femur model and PMHS response to three-point bending drastically decreased when mesh-morphing to SS geometries was applied to the BL model, but the additional inclusion of SS bone modulus did not provide meaningful improvement.

Several lumbar spine biomechanical measurements have been shown to be sensitive to changes in geometry [27-32] and soft tissue implementation [33-34], which could partially explain why HBM response was variable from the PMHS responses in our previous study [18]. Further, considering Park *et al.*'s [22] findings of the importance of SS geometry on femur biomechanical response, a similar approach for the lumbar spine may yield responses closer to those of the PMHS. However, the lumbar spine is more complex than the femur due to the composite structure of bone and soft tissue. The soft tissues have been suggested to play an important role in resisting larger moments [33]. A separate analysis is needed to investigate the effect of geometric specificity on measurement predictions, primarily because differences between SS models of the lumbar spine that represent a wide variation in spinal geometries and soft tissue properties, a BL model of a widely used HBM, and PMHS have not been quantified. We hypothesise that the biomechanical response of the lumbar spine is primarily dictated by the soft tissues (which are not present in the femur), and scaling of these entities will yield the largest effect on response. Therefore, the goals of this study were: (1) to elucidate sensitivity of lumbar spine biomechanical response prediction to SS geometry and scaled soft tissue material properties; and (2) to investigate if predictions of an available HBM lumbar spine improve when one or more of these changes is incorporated.

## II. METHODS

The Global Human Body Model Consortium (GHBMC) HBM (50$^{th}$ percentile detailed male, v6.0.0) was utilised for simulations of PMHS lumbar spines [17] and inclusions of geometric and soft tissue material property variation. Briefly, Tushak *et al.* [17] tested 40 three-vertebrae segments (n=21 T12-L2; n=19 L3-L5). The specimens were quasi-statically, axially compressed to one of three levels (2200 N, 3300 N, 4500 N), and then dynamically flexed at a rate similar to those sustained in frontal MVCs (average peak rate of 600 °/s). Before testing, PMHS spine sections were CT-imaged using a custom, radiopaque jig that positioned specimens in the same initial, neutral posture that was used on the test fixture for biomechanical testing. The PMHS initial positions represented the neutral, unloaded orientation of each spinal section, as estimated using CT scans of the spines in their frozen state upon arrival to the laboratory [17]. The GHBMC lumbar spine vertebrae comprise an outer cortical shell (quadrilateral elements) and inner trabecular bone (hexahedral elements), with ligaments (beam elements) and intervertebral discs (hexahedral and quadrilateral elements) between adjacent vertebrae.

To explore the effects of SS mesh-morphing on biomechanical response, the BL geometry of the GHBMC lumbar spine was used as a Template for morphing to the PMHS geometries, most of which were smaller than the BL model and represented several modes of failure (Tables I and II). The GHBMC lumbar spine segments (T12-L2; L3-L5) were morphed to a subset (n=8) of the PMHS specimens (Table II) to create SS models that represented: (1) geometry close to that of the GHBMC; and (2) the boundaries of variation in geometry among all PMHS specimens. These specimens were chosen to (1) illustrate differences in measurements response that could be due to more than just geometry and (2) provide an indication of the expected level of variability within response. PMHS failure modes included bony fractures and failures at the potting-to-bone interface (Table II). One of the included PMHS did not exhibit any failure, so timing of peak flexion moment was included (M4). In all cases, appropriate censoring was applied to PMHS, as described in [17]. Failure was not defined in the GHBMC, so comparison of model and PMHS responses were only considered until the time of PMHS injury.

Separately, to explore the effects of soft tissue material property definition on biomechanical response, the BL material curves of the ligaments and intervertebral discs were scaled by a few select levels. The soft tissue

properties within the previously tested specimens were not examined, so SS properties were not known. Then, all BL, and SS (geometrically morphed), and scaled (soft tissue properties) models were simulated in matching experimental boundary conditions.

TABLE I
LUMBAR SPINE GEOMETRY

| | T12-L2 Section | | L3-L5 Section | |
|---|---|---|---|---|
| | PMHS | GHBMC | PMHS | GHBMC |
| *CSA[a] ($mm^2$)* | 676 to 1271 | 1180 | 685 to 1598 | 1452 |
| *AP Length[b] (mm)* | 69 to 92 | 78 | 51 to 94 | 81 |
| *VB Height[c] (mm)* | 25 to 29 | 26 | 26 to 32 | 27 |
| *IVD Height[d] (mm)* | 6.3 to 14.2 | 6.2 & 6.9 | 4.5 to 14.9 | 7.6 & 8.1 |
| *Curvature[e] (°)* | -5 to +14 | -12 | +17 to +24 | +14 |

*[a]CSA = vertebral body cross-sectional area of the middle vertebrae.*
*[b]AP = anterior-posterior length of the middle vertebrae.*
*[c]VB Height = vertebral body height of the middle vertebrae.*
*[d]IVD Height = average initial intervertebral disc height of the two discs adjacent to the middle vertebrae.*
*[e]Sagittal curvature of the three-vertebrae segment (negative = kyphotic, positive = lordotic).*

TABLE II
PMHS SPECIMENS SELECTED FOR MORPHING

| Specimen[a] | Section | CSA[b] ($mm^2$) | AP Length[c] (mm) | Curvature[d] (°) | Compression Level (N) | Peak Angular Rate[e] (°/s) | Time of Failure (ms) | Mode of Failure |
|---|---|---|---|---|---|---|---|---|
| M1 | L3-L5 | 1143 | 61 | 24 | 4500 | 652 | 76 | Potting |
| M2 | L3-L5 | 1345 | 94 | 18 | 3300 | 592 | 74 | L4 tear. fx |
| M3 | L3-L5 | 1045 | 85 | 28 | 2200 | 640 | 56 | Potting |
| M4 | T12-L2 | 1205 | 83 | 10 | 4500 | 611 | 109 | None |
| M5 | L3-L5 | 1598 | 78 | 22 | 3300 | 625 | 81 | Potting |
| F1 | T12-L2 | 694 | 77 | 1 | 2200 | 632 | 58 | L1 comp. fx |
| F2 | T12-L2 | 738 | 73 | 9 | 3300 | 585 | 52 | L2 comp. fx |
| F3 | L3-L5 | 792 | 69 | 32 | 3300 | 603 | 52 | L1 comp. fx |

*[a]M = male, F = female.*
*[b]CSA = vertebral body cross-sectional area of the middle vertebrae.*
*[c]AP = anterior-posterior length of the middle vertebrae.*
*[d]Sagittal curvature of the three-vertebrae segment (negative = kyphotic, positive = lordotic).*
*[e]Angular rate was measured for each test from an angular rate sensor located on the rotating potting cup of the experimental test fixture. The relevant test's curve was used as the input pulse to each SS simulation. Peak value occurred at approx. 50 ms.*

***Morphing to Subject-Specific Geometries***

An automated mesh-morphing process, adapted from Park *et al.* [22], was developed to morph the BL GHBMC lumbar spine to match the detailed anthropometry of the selected PMHS specimens (Table II). The morphing process used computed tomography (CT) scans of each specimen in its pre-test initial position. The CT scans of each vertebra were semi-automatically segmented to obtain the stereolithography (STL) surface geometry (Mimics, v21.0, Materialise, Ann Arbor, MI). Due to rough exterior geometry, including small divots, air pockets, and notches, the surface was smoothed (3-matic, v13.0, Materialise; Geomagic Control X, v2017, Oqton, San Francisco, CA) to reveal an exterior that was more user-friendly for morphing, while maintaining the characteristic surface geometry of the vertebrae. The smoothed vertebral geometries were the Target in which to morph the Template BL model. Morphing was then performed using custom MATLAB scripts (2018b, MathWorks, Natick, MA). There were several steps to develop the SS models of each specimen: (1) morphing of outer cortical shell;

(2) morphing of inner trabecular bone; (3) morphing of intervertebral disc; and (4) assembly of the model. Steps 1 and 2 were modified from Park *et al.* [22] to individually morph each vertebra similar to previous morphing of the femur. Then, to account for the compilation of multiple vertebrae in series with soft tissues, Steps 3 and 4 were added.

*Step 1: Morphing of Outer Cortical Shell*

To ensure a similar mesh size between the Template and the Target, and have larger degrees-of-freedom for morphing, the quadrilateral elements from the outer cortical shell were up-sampled into triangular elements by subdividing each quadrilateral into triangles. The node numbers of the original mesh were preserved in the up-sampled mesh, meaning that the nodes representing the original corners of the quadrilateral elements retained their node numbers. Triangular elements were necessary to morph the cortical shell without the use of control points. The first step of the cortical shell morphing was a manual alignment of the Template to match the spatial orientation of the Target using a vertebral body coordinate system (defined using Wu *et al.* [35]). Next, both geometries were centered and rigidly transformed using an iterative closest point (ICP) algorithm [36]; the ICP algorithm determined a rigid body transformation, which aligned the Template geometry to the Target geometry by finding the closest points in the Target geometry to the Template geometry. After applying the ICP, the Target was scaled in the three directions along the principal axes to match size between the two geometries. The scaled Template was then morphed to further minimise the error at each node between the Template and the Target geometries following Burr's elastic registration algorithm [37]. An error tolerance of 0.25 mm was employed, which was the maximum allowable nodal distance error for the code to converge. A normal vector search was implemented such that Template to Target node mapping was not allowed on neighbouring surfaces that could cause spinal canal collapse. After morphing the cortical surface, the nodal coordinates of the up-sampled mesh were exported into a keyword file following the LS-DYNA format. The nodal coordinates of the original Template nodes were updated based on the nodal coordinates of the final morphed model to maintain the original number of elements. Therefore, up-sampling was employed solely to achieve geometrical accuracy in morphing and not carried through into the final cortical mesh.

*Step 2: Morphing of the Inner Trabecular Bone*

Each node from the morphed outer cortical shell was selected as a control point to morph the inner trabecular hexahedral elements. This was possible because both the outer cortical quadrilateral elements and inner trabecular hexahedral elements share nodes on the exterior surface of the trabecular bone. Using the transformation matrix obtained in Step 1, the trabecular bone was positioned to match the rough spatial orientation of the Target. Finally, with selected control points, the geometry of the Template trabecular bone was transformed to the Target geometry of each specimen using a morphing technique that implemented a thin-plate spline with a radial basis function, an extension of the original thin-plate spline proposed by Bookstein [38], to account for landmark localisation errors [39]. The accuracy of the developed SS model was evaluated using the average minimum distance error (the average distance between the nodes on the surface of the morphed SS model and the surface of the Target, with an allowable 0.25 mm tolerance). Morphing the Templates using the pre-test CT scans as Targets ensured the positioning of the GHBMC spinal segments in corresponding pre-test positions.

*Step 3: Morphing of Intervertebral Discs*

The intervertebral discs (IVDs) of the GHBMC are comprised of the annulus, fibrosus, and nucleus modelled as three different parts. Similar to the trabecular bone, the IVDs share nodes with adjacent cortical endplates. For the purpose of morphing, all IVD parts were treated together as one entity. The top and bottom surfaces of the IVDs were chosen as the control points to morph each IVD using the same methodology as in Step 2.

*Step 4: Assembly of the Models*

The nodal coordinates of the input files in the above steps were updated after the morphing process was completed. The result was SS models with the same node, element, and part identification as the BL model, with the only difference among models being the geometry. It should be noted that the ligament attachment locations in the BL model are determined by specific node numbers, and those node numbers were maintained after

morphing was completed. No effort was made to adjust attachment locations of the ligament beam elements during the morphing process due to the lack of PMHS ligament position data.

***Scaling Soft Tissue Material Properties***

The existing ligament and IVD material stiffness definitions in the BL model were arbitrarily scaled up and down by a quarter and a half of the original (50%, 75%, 125%, and 150%). The ligaments in the GHBMC are characterised by force-elongation curves with three points connected by lines (Fig. 1). The force-elongation curves are applied to each ligament fiber bundle (beam element), with fiber bundles in a ligament acting as springs in parallel. Scale factors were individually applied to all soft tissue entities except for the anterior longitudinal ligament since it does not participate in resisting flexion motion. All three y-values were scaled by each of the four levels, while the corresponding three x-values were unchanged (Fig. 2), thereby scaling the total effective tensile force in the whole ligament enough to hypothetically elicit notable changes in mechanical behavior. In return, the stiffness characterising each of the regions within the curves was increased or decreased. Then, to demonstrate the effect of extreme changes, all ligament material properties were scaled up and down by 50%, compounding individual effects from each ligament. The stiffness of the two components of the IVD in the GHBMC are not defined with curves, but rather have material definitions appropriate for incompressible fluids (nucleus pulposus) and elastic (annulus fibrosus). Consequently, the bulk modulus of both IVD components was scaled by each of the four levels, either increasing or decreasing the stiffness.

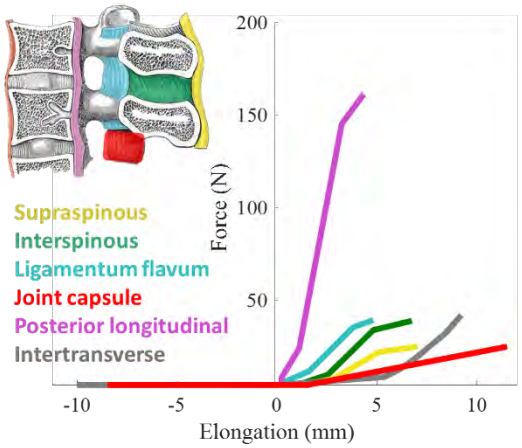


Fig. 1. Ligament material curves, applied on a per beam element basis, for the six essential ligaments resisting flexion motion.

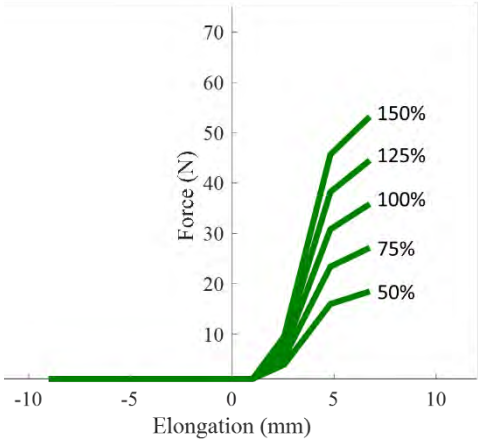


Fig. 2. Example of scaling the y-axis force values for the interspinous ligament by +/- 25% and 50%.

***Simulations of All Models in Experimental Boundary Conditions***

Simulations of all models were performed to assess the differences in biomechanical response when geometry and soft tissue material properties were varied, totaling 59 simulations (LS-DYNA, R12.0.0, mpp971, ANSYS, Canonsburg, PA). The simulation setup was the same as that described in Tushak *et al.* [18] to represent a simplified test fixture and the experimental boundary conditions (Fig. 3). The three-vertebrae section was secured between two potting cups, where the bottom potting cup was constrained in all but anterior-posterior and superior/inferior translation. The input pulse (flexion angular velocity) was prescribed to the top potting cup to act about a reference rigid body with a cylindrical joint definition (centre of rotation). A global axial compression force was applied perpendicular to the mid-plane of the middle vertebrae at the beginning, and maintained for the duration of the simulation (200 ms), to mimic experimental conditions and reduce off-axis loading.

For the eight SS models, input pulse and axial compression level (Table II) was specific to the corresponding PMHS test. Additionally, the BL geometry T12-L2 or L3-L5 section was simulated with these boundary conditions for equal comparison with regard to all factors other than geometry. It should be noted that morphing to SS geometries automatically positioned the three-vertebrae segment to its pre-test initial position, which was approximated to be a neutral, unloaded position in the experiments [17]. Thus, pre-stresses and pre-strains were set to zero in the simulations.

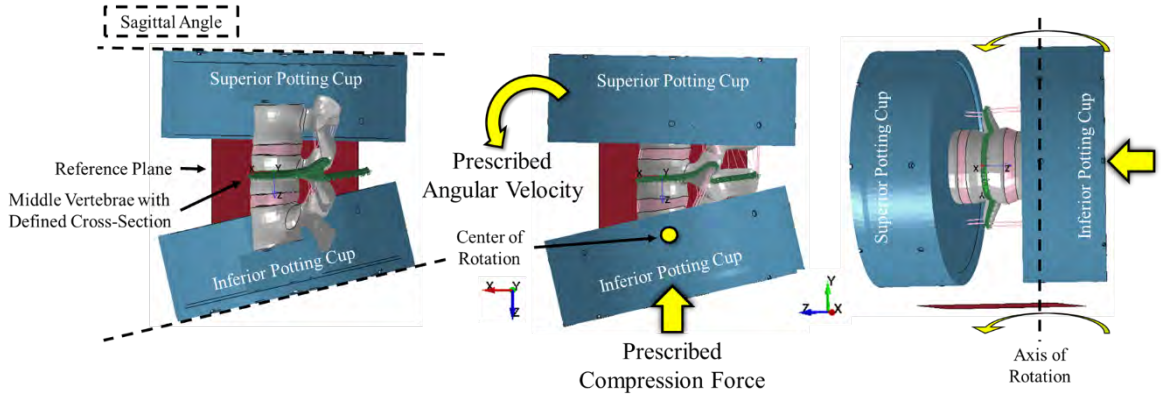


Fig. 3. Simulation setup with the middle vertebrae cross-section and global coordinate systems, in which the principal axes were aligned.

For the cases of soft tissue material property scaling, only one lumbar section (L3-L5) in the occupant posture was simulated at the middle level of axial compression (3300 N) since Tushak *et al.* [18] found that moment-angle responses and stiffness (slope of the response) for both sections and all three levels of axial compression were similar across seating postures. An averaged input pulse was used for the simulations with soft tissue scaling, same as Tushak *et al*. [18]. Again, pre-stresses and pre-strains were set to zero in the simulations to mimic the PMHS initial loading state.

A one-element-thick continuous cross-section was defined in the middle vertebrae for measuring loads analogous to the methods in the experiments (Fig. 3). Loads for the duration of the simulation were reported with respect to the middle vertebrae coordinate system for comparison to the corresponding PMHS loads. When doing this, the flexion moment was adjusted for the measured axial compression force multiplied by its moment arm between the centroid of the defined cross-section and the centre of the middle vertebrae vertebral body. The sagittal angle of the top potting cup relative to its initial position (global flexion rotation angle of the three-vertebra section) was extracted to compare flexion moment-angle response until the point of PMHS failure.

## III. RESULTS

The eight SS models displayed clear differences in several aspects of geometry compared to the BL geometry, including gross vertebral size (694–1598 mm$^2$ CSA, 61–94 mm anterior-posterior length), local anatomical variation in bone landmarks, and spinal curvature (1–32° lordosis) (Fig. 4). The three-vertebra models achieved a morphing error of less than 0.25 mm compared to the Target segmented CT scans, and each was developed in less than an hour.

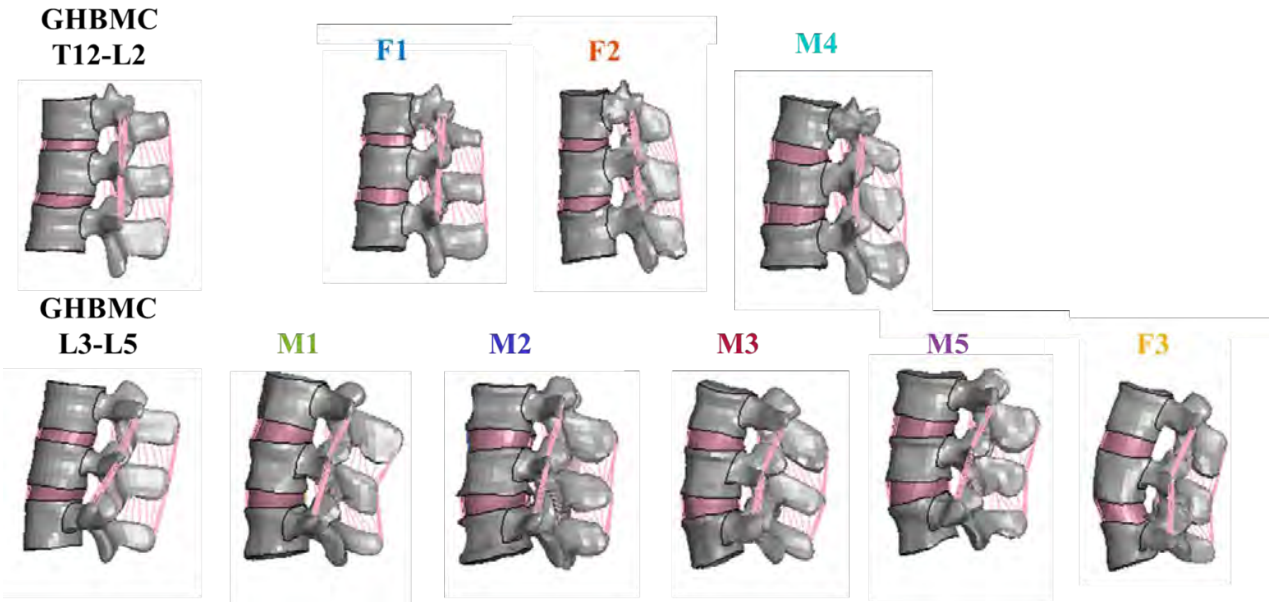


Fig. 4. BL GHBMC models and SS models resulting from morphing. All models are shown on the same scale to visualise relative differences in geometry and size.

The biomechanical responses of the GHBMC lumbar spine segments were relatively insensitive to changes in geometry (Fig. 5) (up to 16% variation of peak moment from the BL). Best-fit slopes representing stiffness were not significantly different between BL and SS cases (BL mean = 2.49 Nm/deg, SS mean = 2.39 Nm/deg). In some cases, morphing to SS geometries caused increased initial extension moment upon the application of axial compression at the beginning of the simulations (986U, 968L, 986L), although the stiffness of the response remained similar between models regardless of the initial offset moment. Differences in flexion moments for every given flexion angle among models and PMHS were observed, particularly at the time of failure (Fig. 5). Additionally, individual changes in soft tissue properties largely did not affect biomechanical response (Fig. 6). However, the combined effect of scaling all ligaments was greater than both individual scaling and morphing (25% variation of peak moment from the BL). All models captured the experimental response at low angles (~15° and less; selected females), but all models also deviated from experiments at higher angles and moments due to the differences in response behaviour (linear GHBMC vs. bilinear PMHS).

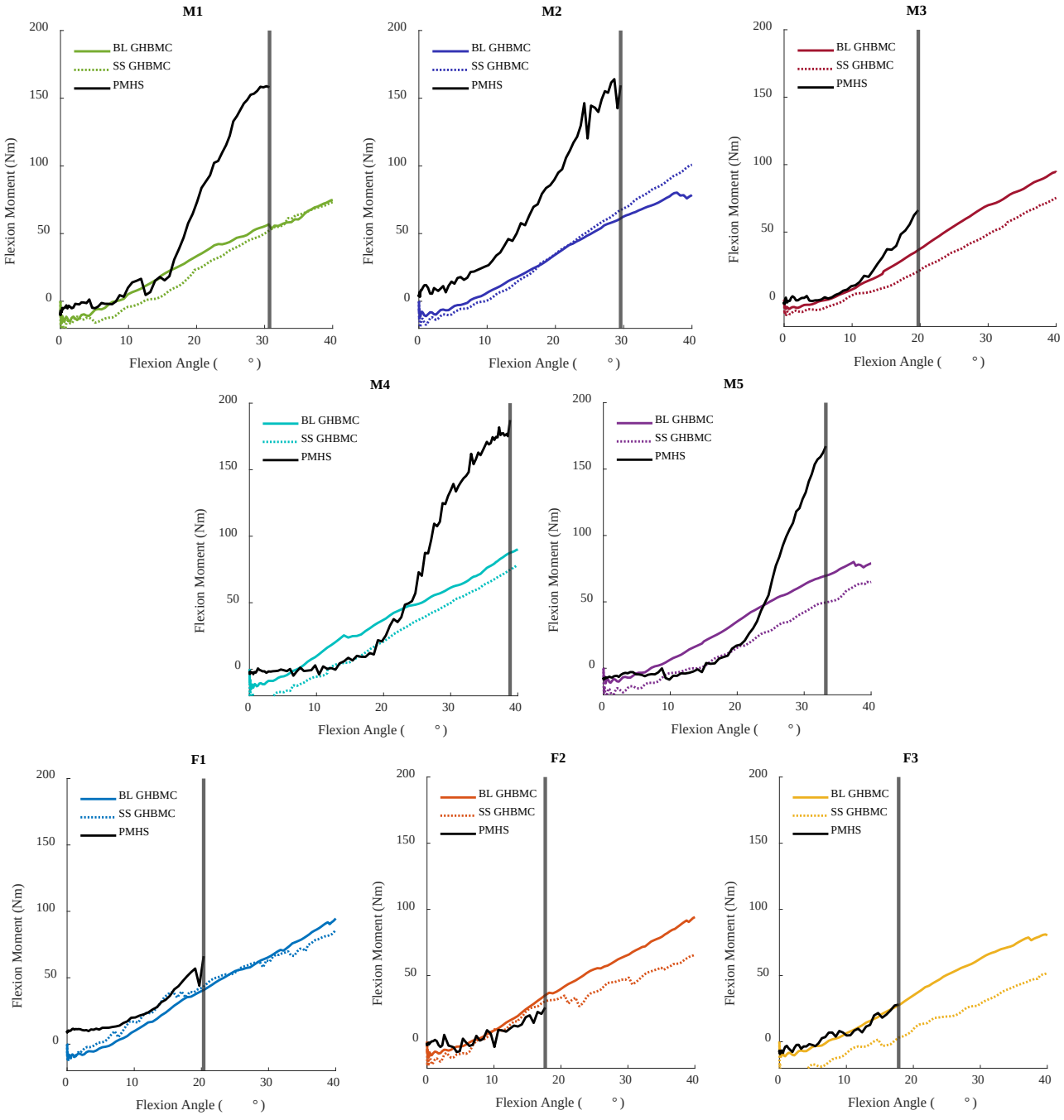


Fig. 5. Flexion moment-angle responses by model type (BL = baseline, solid; SS = subject-specific, dashed). Colour indicates specimen. Vertical grey lines indicate the PMHS times of failure (failure type included in Table II).

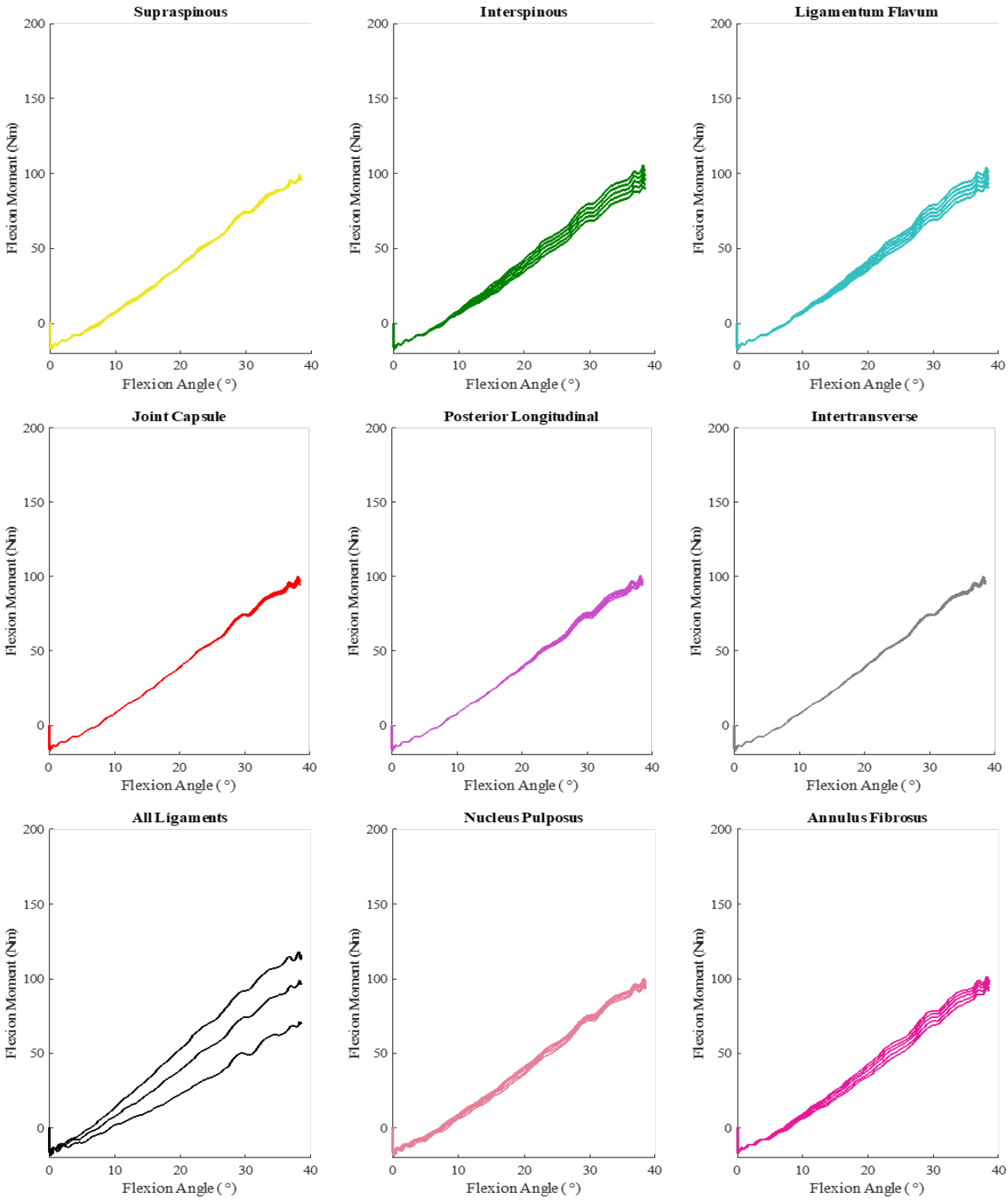


Fig. 6. Flexion moment-angle responses by soft tissue scaling. Curves resulting from all scale factors of each soft tissue entity plotted together.

## IV. DISCUSSION

The morphing process proved to be robust when adapted for the lumbar spine and applied to the subset of eight specimens: the chosen specimens represented the largest variations within donor vertebrae geometry and size, and the larger specimens had geometry closest to that of the GHBMC. When morphing the Template quadrilateral elements to the Target geometry, the Template mesh density was increased (triangular elements) to better match the mesh density of the STL and remove the need for defining traditional control points or landmarks, which are commonly used in other morphing methods for the lumbar spine [20][40-42]. Rather, a

more efficient process was utilised in which the Template surface was deformed onto the Target surface such that the distance between surface vertices was minimised. The act of globally transforming and scaling the Template before the elastic registration step reduced the time needed and error associated with elastic registration due to the two surfaces being closer to each other in space.

After morphing the triangular elements, the mesh density was then decreased compared to the original level (quadrilateral). The SS versions of the GHBMC lumbar spine contained the same node, element, part, and material numbers and IDs, so there is the potential to insert SS model(s) into a larger component or full-body of the GHBMC. This morphing method was adapted from previous efforts for the femur [22], so this morphing technique may be suitable for other entities, from long bones (e.g. tibia, humerus, etc.) to potentially more complex structures akin to the spine (e.g. rib cage). Additionally, because the cortical bone quadrilateral elements and the trabecular bone hexahedral elements share node numbers in the GHBMC model, it was possible to use the node numbers as control points to easily morph the hexahedral elements. Further, in the GHBMC the endplates of the vertebrae and adjacent IVDs share nodes to similarly morph the IVDs. In the case that the chosen HBM does not share nodes between entities, the morphing has to be performed in the following two steps. First, identify the adjacent surface's nodes (i.e. of the cortical shell) to the desired entity (i.e. IVDs) to act as a Target. Then, the updated control points of the adjacent entity from Step 1 (i.e. cortical shell) can be used to morph the desired entity using the thin-plate spline methodology.

The practice of evaluating SS models relative to both their relevant PMHS data and a BL model is valuable but has not been common. However, it was successfully performed for the lumbar spine. The GHBMC captured the PMHS response at low angles and moments (~10° and less), which was likely representative of the range of motion and not necessarily bending angles that approach failure. The majority of all PMHS responses were bilinear (n=31 bilinear, n=3 linear) [17]. The BL model did not capture the stiffening occurring at 10–15° in the majority of the PMHS, and the introduction of SS geometry did not substantially result in the stiffening behaviour. However, the GHBMC matched the PMHS specimens that demonstrated primarily linear responses. These PMHS were segments from female subjects that failed earlier from vertebral body compression fractures, with generally small geometry compared to the GHBMC. The PMHS with geometry most similar to the GHBMC (males) yielded dissimilar responses and moments at time of PMHS failure, some of which were bony fractures and others were interface failures or no failure at all, primarily because bilinear behaviour was absent in the GHBMC. A potential culprit of the discrepancy may be the soft tissue materials. There is difference in the human's and GHBMC's ability to maintain intervertebral disc height and volume at high deformations (Fig. A1). The GHBMC lost approximately 20-40% of its height after axial compression was applied and over 80% by 20° of flexion. Additionally, ligaments were stretched past the deflection limits of their curve definitions, indicating more elongation than in humans (Fig. A2). Ligament stretch could have been a direct consequence of disc collapse. Thus, addressing the material models of the disc and/or ligaments may provide the greatest benefit to mechanical response behavior. Additionally, some SS models had initial extension moments in the spinal segment caused by the application of axial compression, which indicated that the axial compression was not applied perpendicular to the mid-plane of the middle vertebrae. However, regardless of the initial extension moments, the resulting responses had similar stiffness. There also appeared to be no clear trend between spinal curvature and response, potentially because all simulations began in zero-stress states.

Further, while less difference was observed in global biomechanical response between BL and SS geometries, larger changes might be illustrated for material metrics in future analysis. Changes in geometry have been shown to result in drastic differences in internal biomechanics, while the global behaviour may be relatively similar [29]. Thus, it may be important to evaluate both measurements to better understand the structure on both a global and local scale. Previous studies that have elucidated sensitivity of lumbar spine biomechanics to geometry used FE modelling [28-32] with quasi-static, physiologic loading rather than high-rate, injurious loading. Therefore, loading rate dependencies and engagement of ligaments past their passive range of motion may outweigh the effects of geometrical differences. Additionally, soft tissues have been suggested to play an important role in resisting larger moments [33], so the soft tissues may have a larger effect on biomechanical response than bony geometry at the level of loading implemented in this study. Lastly, degradation of bone associated with aging affects bone structure and one's ability to bear load but was not assessed in this study.

Ultimately, if the highest level of predictive accuracy is desired for a HBM, enough specificity should be included in the model formulation to capture the variation within the population while yielding the simplest

formulation to capture that variation. Therefore, the sensitivity of the BL model to SS parameters that are most likely to affect biomechanical measurements of interest should be assessed to evaluate the benefit of including more specificity in the model and to verify that the endeavour of obtaining the SS data will be warranted. When assessed over the largest possible range, the version of the GHBMC utilised in this study, despite including SS geometry, only served to introduce unnecessary complexity without providing improvement in predicting the biomechanical response. On the other hand, combined changes to ligament material properties provided larger distinctions among biomechanical responses. Effort may be better served in addressing the soft tissue formulations to improve model biofidelity. After that, the effect of SS geometry may be reassessed. Alternatively, it is probable that the soft tissues within the composite structure of the lumbar spine largely dictate biomechanics, and the effects of changes in gross bony geometry are downsized in comparison.

## V. CONCLUSION

A published technique was adapted for morphing CT scans of the lumbar spine to create eight geometrically variable subject-specific models stemming from the GHBMC BL. The biomechanical responses of the BL and SS GHBMC lumbar spine sections were insensitive to changes in geometry and soft tissue stiffness and under-predicted flexion moments at higher flexion angles (relative to their PMHS counterpart). The BL model yielded similar prediction capability as the modified models when subjected to the boundary conditions included in this study. Therefore, the added complexity and effort of incorporating SS geometries was not fruitful for this HBM in this loading condition, but systemic modifications to soft tissues are promising.

## VI. ACKNOWLEDGEMENTS

This work was supported by Autoliv Research. It should be noted that the views or opinions expressed here are those of the authors and not necessarily aligned with the views and opinions of the sponsoring organisation.

## VII. REFERENCES

[1] Doud, A. N,, Weaver, A. A , *et al*. (2015) Has the incidence of thoracolumbar spine injuries increased in the United States from 1998 to 2011? *Clinical Orthopaedics and Related Research*, **473**(1): pp. 297–304.

[2] Pintar, F. A., Yoganandan, N., Maiman, D. J., Scarboro, M., Rudd, R. W. (2012) Thoracolumbar spine fractures in frontal impact crashes. Annals of advances in automotive medicine. *Proceedings of the Annual Scientific Conference of the Association for the Advancement of Automotive Medicine*, , **56**:pp. 277–283.

[3] Kaufman, R. P., Ching, R. P., *et al*. (2013) Burst fractures of the lumbar spine in frontal crashes. *Accident Analysis & Prevention*, **59**: pp. 153–163.

[4] Wang, M. C., Pintar, F. A., Yoganandan, N., Maiman, D. J. (2009) The continued burden of spine fractures after motor vehicle crashes. *Journal of Neurosurgery: Spine*, **10**: pp. 86–92.

[5] Boyle, K. J., Reed, M. P., Zaseck, L. W., Hu, J. (2019) A Human Modelling Study on Occupant Kinematics in Highly Reclined Seats during Frontal Crashes. *Proceedings of the IRCOBI Conference*, 2019, Florence, Italy.

[6] Rawska, K., Gepner, B. D., *et al.* (2019) Submarining sensitivity across varied anthropometry in an autonomous driving system environment. *Traffic Injury Prevention*, **20**(sup2): pp. S123–S127.

[7] Tang, L., Zheng, J., Hu, J. (2020) A numerical investigation of factors affecting lumbar spine injuries in frontal crashes. *Accidental Analysis & Prevention*, **136**(105400).

[8] Forman, J. L., Lin, H., Gepner, B. D., Wu, T., Panzer, M. B. (2019) Occupant Safety in Automated Vehicles-Effect of Seatback Recline on Occupant Restraint. *International Journal of Automotive Engineering*, **10**(2): pp. 139–143.

[9] Gepner, B. D., Draper, D., *et al.* (2019) Comparison of Human Body Models in Frontal Crashes with Reclined Seatback. *Proceedings of the IRCOBI Conference*, 2019, Florence, Italy.

[10] Adams, M. A., Dolan, P. (2011) Biomechanics of vertebral compression fractures and clinical application. *Archives of Orthopaedic and Trauma Surgery*, **131**: pp. 1703–1710.

[11] Holdsworth, F. W. (1963) Fractures, Dislocations, and Fracture-Dislocations of the Spine. *Journal of Bone and Joint Surgery*, **45**(1): pp. 1534–1551.

[12] Rao, R. D., Berry, C. A., Yoganandan, N., Agarwal, A. (2014) Occupant and crash characteristics in thoracic and lumbar spine injuries resulting from motor vehicle collisions. *Spine*, **14**(10): pp. 2355–2365.

[13] Roaf, R. (1960) A study of the mechanics of spinal injuries. *Journal of Bone and Joint Surgery*, **42**: pp. 810–

823.
[14] Shaikh, J., Thathia, H., Lubbe, N. (2020) Lumbar Spine Injuries in Motor Vehicle Crashes. *Proceedings of the IRCOBI Conference*, 2020, Beijing, China.
[15] Tran, N. T., Watson, N. A., Tencer, A. F., Ching, R. P., Anderson, P. A. (1995) Mechanism of the burst fracture in the thoracolumbar spine: the effect of loading rate. *Spine*, **20**(18): pp. 1984–1988.
[16] Crandall, J. R., Bose, D., *et al*. (2011) Human surrogates for injury biomechanics research. *Clinical anatomy*, **24**(3): pp. 362–371.
[17]Tushak, S. K., Donlon, J. P., *et al*. (2022) Failure Tolerance of the Human Lumbar Spine in Dynamic Combined Compression and Flexion Loading. *Journal of Biomechanics*, **135**: 111051.
[18] Tushak, S. K., Gepner, B. D., Pipkorn, B., Kerrigan, J. R. (2022) Evaluation of the GHBMC Lumbar Spine in Sub-injurious and Injurious Loading. *Proceedings of the IRCOBI Conference*, 2022, Porto, Portugal.
[19] Anderson, A. E., Peters, C. L., Tuttle, B. D., Weiss, J. A. (2005) Subject-Specific Finite Element Model of the Pelvis: Development, Validation and Sensitivity Studies. *Journal of Biomechanical Engineering*, **127**(3): pp. 364–373.
[20] Campbell, J. Q., Petrella, A. J. (2015) An automated method for landmark identification and finite-element modeling of the lumbar spine. *IEEE Transactions on Biomedical Engineering*, **62**(11): pp. 2709–2716.
[21] Iraeus, J., Lundin, L., *et al.* (2019) Detailed subject-specific FE rib modeling for fracture prediction. *Traffic Injury Prevention*, **20**(sup2): pp. S88–S95.
[22] Park, G., Kin, T., Forman, J., Panzer, M. B., Crandall, J. R. (2017) Prediction of the structural response of the femoral shaft under dynamic loading using subject-specific finite element models. *Computer methods in biomechanics and biomedical engineering*, **20**(11): pp. 1151–1166.
[23]Li, Z., Kindig, M. W., Kerrigan, J. R., Kent, R. W., Crandall, J. R. (2013) Development and Validation of a Subject-Specific Finite Element Model of a Human Clavicle. *Computer Methods in Biomechanics and Biomedical Engineering*, **16**(8): pp. 819–829.
[24]Li, Z., Kindig, M. W., Subit, D., Kent, R. W. (2010) Influence of mesh density, cortical thickness and material properties on human rib fracture prediction. *Medical engineering & physics*, **32**(9): pp. 998–1008.
[25] O'Reilly, M. A., Whyne, C. M. (2008) Comparison of computed tomography based parametric and patient-specific finite element models of the healthy and metastatic spine using a mesh-morphing algorithm. *Spine*, **33**(17): pp. 1876–1881.
[26] Turbucz, M., Pokorni, A. J., *et al.* (2022) Development and Validation of Two Intact Lumbar Spine Finite Element Models for In Silico Investigations: Comparison of the Bone Modelling Approaches. *Applied Sciences*, **12**: 10256.
[27] Campbell, J., Petrella, A. J. (2016) Automated finite element modeling of the lumbar spine: using a statistical shape model to generate a virtual population of models. *Journal of Biomechanics*, **49**(13): pp. 2593–2599.
[28] Niemeyer, F, Wilke, H. J., Schmidt, H. (2012) Geometry strongly influences the response of numerical models of the lumbar spine—a probabilistic finite element analysis. *Journal of Biomechanics*, **45**(8): pp. 1414–1423.
[29] Noailly, J., Wilke, H. J., Planell, J. A., Lacroix, D. (2007) How does the geometry affect the internal biomechanics of a lumbar spine bi-segment finite element model? Consequences on the validation process. *Journal of Biomechanics*, **40**(11): pp. 2414–2425.
[30] Natarajan, R. N., Andersson, G. B. (1999) The influence of lumbar disc height and cross-sectional area on the mechanical response of the disc to physiologic loading. *Spine*, **24**(18): p. 1873.
[31] Meijer, G. J., Homminga, J., Veldhuizen, A. G., Verkerke, G. J. (2011) Influence of interpersonal geometrical variation on spinal motion segment stiffness: implications for patient-specific modeling. *Spine*, **36**(14): pp. E929–E935.
[32] Putzer, M., Ehrlich, I., Rasmussen, J., Gebbeken, N., Dendorfer, S. (2016) Sensitivity of lumbar spine loading to anatomical parameters. *Journal of Biomechanics*, **49**(6): pp. 953–958.
[33] Naserkhaki, S., Arjmand, N., Shirazi-Adl, A., Farahmand, F., El-Rich, M. (2018) Effects of eight different ligament property datasets on biomechanics of a lumbar L4-L5 finite element model. *Journal of Biomechanics*, **70**: pp. 33–42.
[34] Wiczenbach, T., Pachocki, L., Daszkiewicz, K., Luczkiewicz, P., Witkowski, W. (2023) Development and validation of lumbar spine finite element model. PeerJ, DOI10.7717/peerj.15805.
[35]Wu, G., Siegler, S., *et al.* (2002) ISB recommendation on definitions of joint coordinate system of various joints

for the reporting of human joint motion—part I: ankle, hip, and spine. *Journal of Biomechanics*, **35**(4): pp. 543–548.

[36] Besl, P. J., McKay, N. D. (1992) Method for registration of 3-D shapes. Sensor fusion IV: control paradigms and data structures. *IEEE Transactions on Pattern Analysis and Machine Intellegence*, **14**(2): pp. 239-256.

[37] Bryan, R., Mohan, P. S., *et al*. (2010) Statistical modelling of the whole human femur incorporating geometric and material properties. *Medical Engineering & Physics*, **32**(1): pp. 57–65.

[38] Bookstein, F. L. (1989) Principal warps: Thin-plate splines and the decomposition of deformations. *IEEE Transactions on pattern analysis and machine intelligence*, **11**(6): pp. 567–585.

[39] Rohr, K., Stiehl, H. S., *et al*. (2001) Landmark-based elastic registration using approximating thin-plate splines. *IEEE Transactions on medical imaging*, **20**(6): pp. 526–534.

[40] Lalonde, N. M., Petit, Y., Aubin, C. E., Wagnac, E., Arnoux, P. J. (2013) Method to geometrically personalize a detailed finite-element model of the spine. *IEEE Transactions on Biomedical Engineering*, **60**(7): pp. 2014–2021.

[41] Sigal, I. A., Hardisty, M. R., Whyne, C. M. (2008) Mesh-morphing algorithms for specimen-specific finite element modelling. *Journal of Biomechanics*, **41**: pp. 1381–1389.

[42] Tang, L., Hu, Z., Lin, Y. S., Hu, J. (2022) A statistical lumbar spine geometry model accounting for variations by Age, Sex, Stature, and body mass index. *Journal of Biomechanics*, **130**: 110821.

**Appendix A: GHBMC soft tissue illustrations**

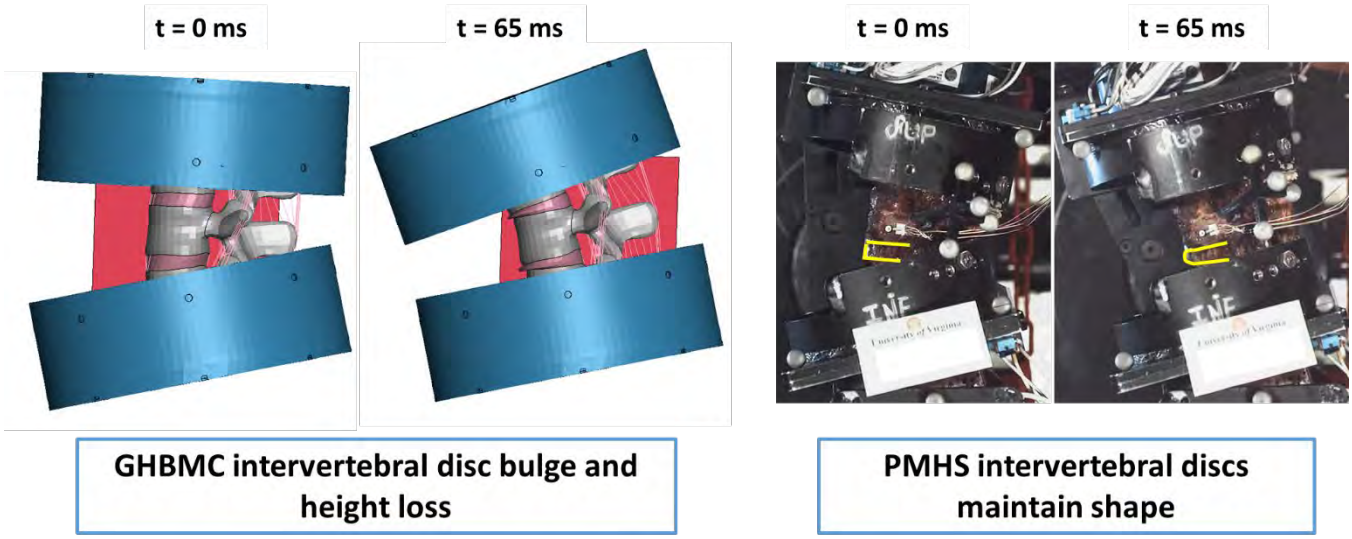


Fig. A1. Illustration of GHBMC intervertebral disc behavior compared to that of PMHS, with initial orientation and structure at 20 degrees of flexion.

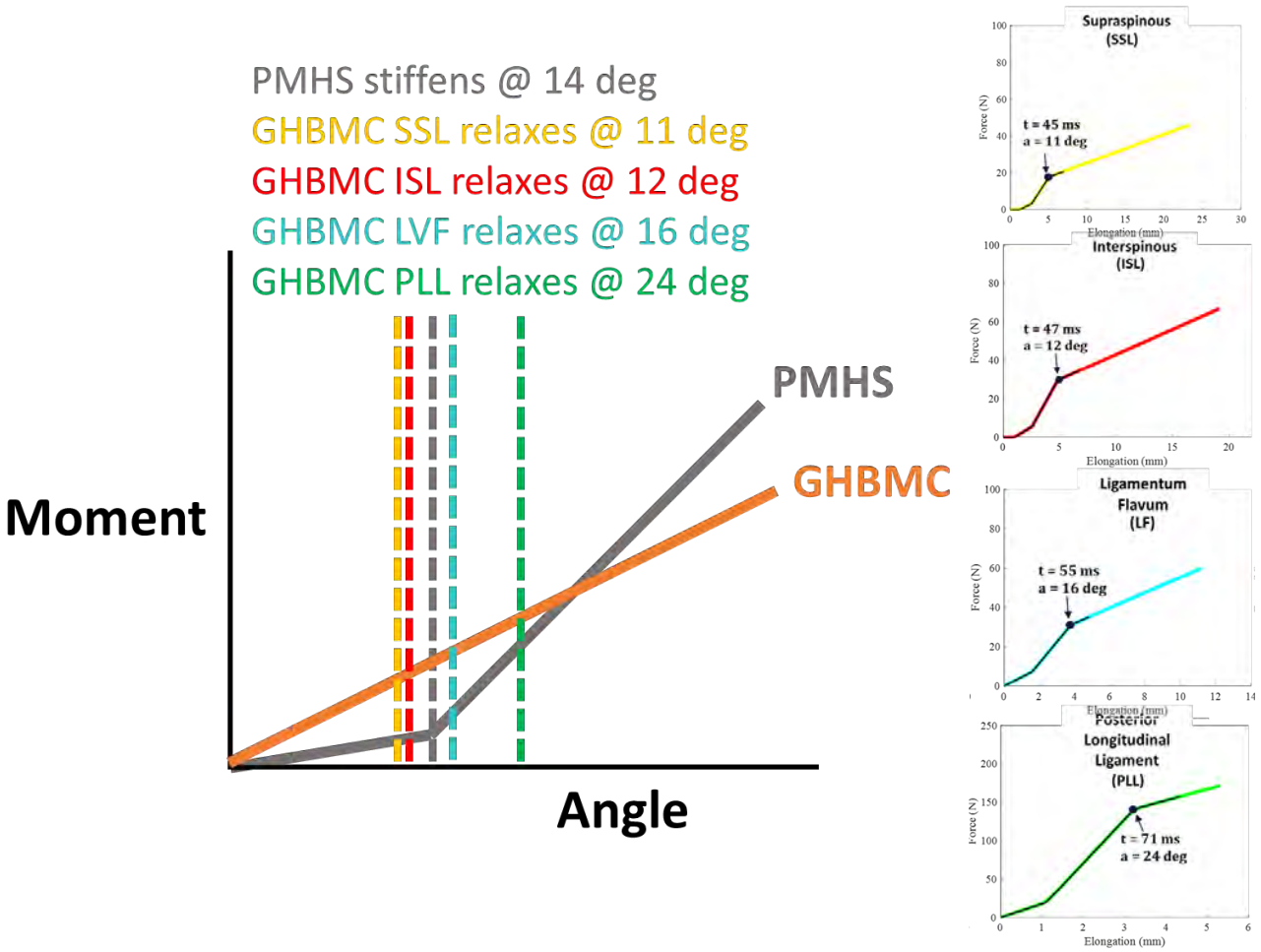


Fig. A2. Left: Exemplary response behavior for the GHBMC (orange) and PMHS (grey), with vertical lines indicating the typical angle of inflection for when PMHS stiffen (dashed grey) and the angles at which each GHBMC ligament enters the strain-softening region of the material curve definition (gold, red, blue, and green). Right: The corresponding original ligament definition curves for the GHBMC (black), along with the force and elongation measured in the GHBMC supraspinous (gold), ligamentum flavum (blue), posterior longitudinal ligament (green), and interspinous (red) ligaments. The curves depict responses of one fiber bundle (i.e. one beam element) of each of the four ligaments. The force and elongation of the ligaments extend past the ligaments' original definition.